Unsupervised domain adaptation for GPM satellite constellation using CycleGAN

Vibolroth Sambath[1]*, Nicolas Viltard[1], Laurent Barthès[1], Audrey Martini[1] and Cécile Mallet[1]
[1]Laboratoire ATmosphères, Milieux et Observations Spatiales (LATMOS), Guyancourt, 78280, France
*Corresponding author. Email: vibolroth.sambath@latmos.ipsl.fr

Introduction

- The estimation of precipitation for a given date and location is a very challenging task because rain is very intermittent in time and space. Ground-based observations alone could be insufficient. On the other hand, satellite observations have an advantage in global coverage (Hou et al., 2014).
- The Global Precipitation Mission (GPM) Core satellite, with the objective of providing uniform global precipitation, measures the microwave brightness temperature (GMI) and a more direct observation of rain rates with the precipitation radar (DPR).
- Using these data, Viltard et al. (2020) developed a deep learning model using U-Net (Ronneberger et al., 2015) for rain retrieval (DRAIN).
- However, the other satellites within the constellation do not contain the collocated brightness temperature and rain rates for a supervised rain retrieval approach. They also have slightly different configurations.

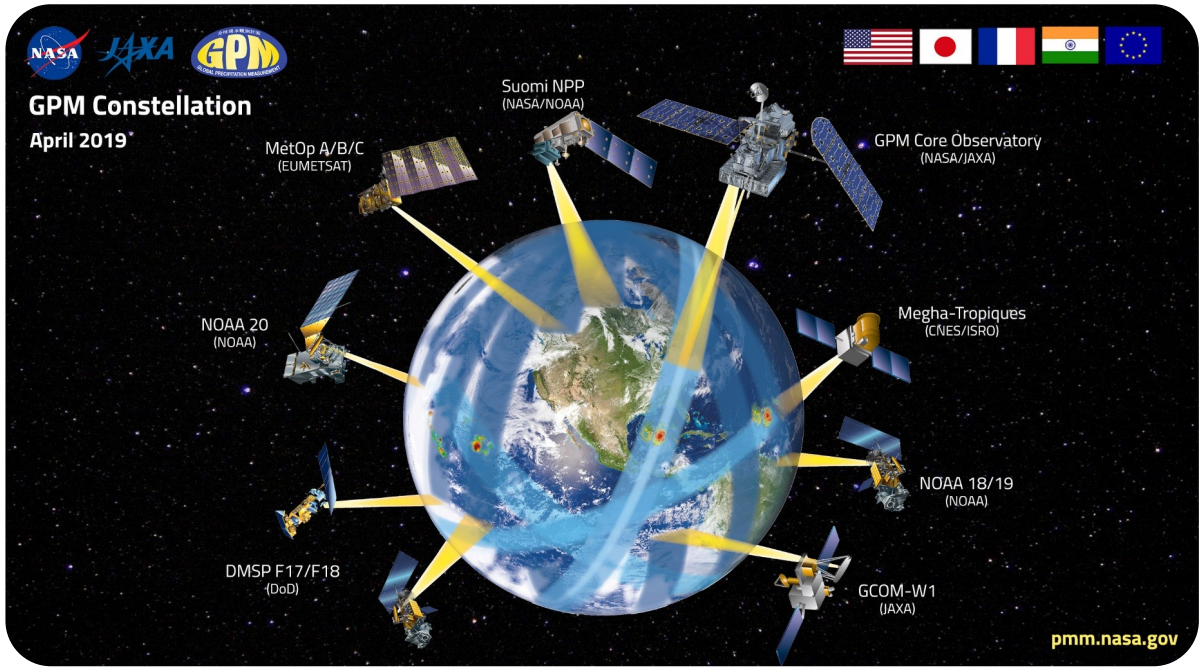

Figure 1. The Global Precipitation Mission (GPM) Constellation as of early 2019. Each satellite member in the constellation has its own scientific objective though they all contribute to the pasive microwave brightness temperature measurement. (GPM website).

Objective

- Use CycleGAN, an unsupervised domain adaptation method, to adapt between different source and target domains of satellite observations in order to apply a pre-trained (on the source domain) rain retrieval model.

Method

- CycleGAN is an image transformation method that does not require paired database. It consists of two GANs working together, each containing a generator and a discriminator (Zhu et al., 2017a).
- The first generator G takes an image from the source domain X and transforms it into the target domain Y . The second generator F works the other way around, by transforming an image in Y into X. The discriminators D_X and D_Y try to correctly label if a sample is from its respective domain.
- The discriminators loss is its ability to distinguish fake and real images.
- Each generator has three terms of loss: cycle-consistency loss, identity loss and adversarial loss.
  - Cycle consistency: a complete image transformation cycle (from X to Y and back to X) should be comparable to the original image.
  - Identity loss: the difference between an image and the transformation to its own domain ($\| F(x) - x \|_1$).
  - Adversarial loss: working against the descriminators as in Generative Adversarial Networks (GAN) (Goodfellow et al., 2014).

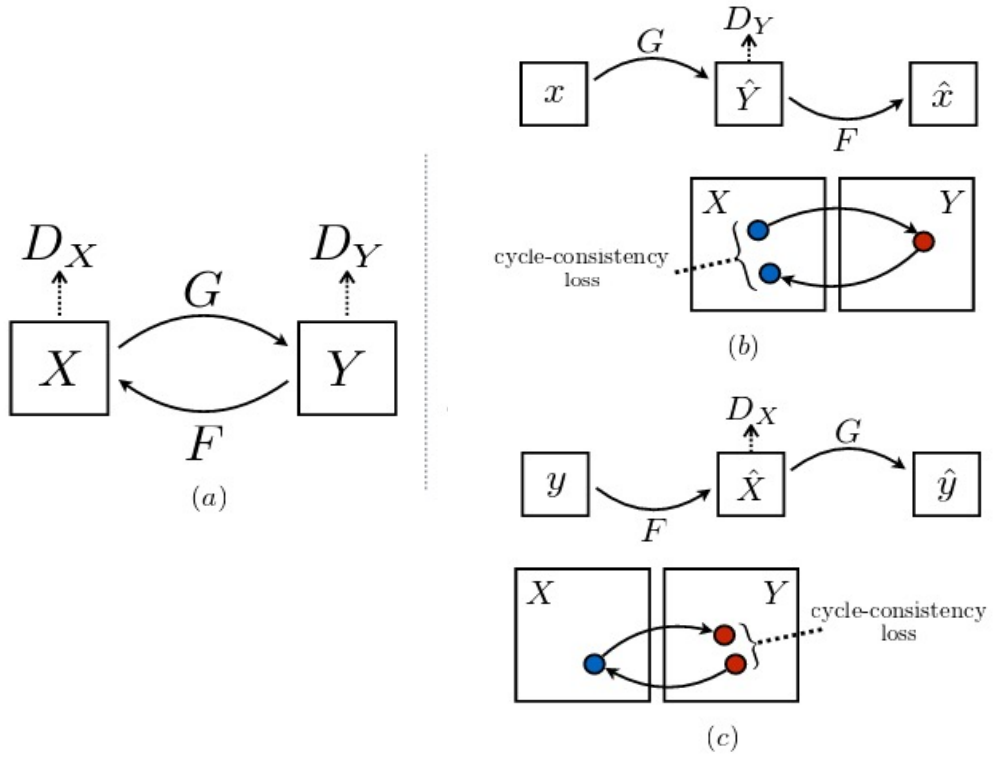

Figure 2. The architecture of CycleGAN. (b) and (c) cycle-consistency loss. (Zhu et al., 2017a).

Training details

- U-Net is used as the generators due to its efficiency in dealing with GMI data (Viltard et al. 2020).
- Different learning rate decays help balance the loss between the two domains.
- With numerous testing, smaller batch size performs better.

Data

- The GPM Microwave Imager (GMI) is a multi-channel conically scanning radiometer with a swath of 904 km and with channels ranging from 10 GHz to 183 GHz. These channels are measured in both Horizontal (H) and Vertical (V) polarization.
- 89 GHz observations in V and H are used in this study.
- The difference between 89H and V is mostly due to the surface emissivity difference between the two channels with the V surface emissivity almost always higher than the H, leading to a generally higher V brightness temperature. However, polarisation due to scattering by ice might occur in (rare) cases of oriented particles leading to a H brightness temperature higher than V. This is true for both land and ocean situations.

Pre-processing

- Then, the images are normalized, randomly cropped to 128x128 pixels, and randomly rotated.
- The random crop and random rotation are applied in order to increase the difficulty of the task.

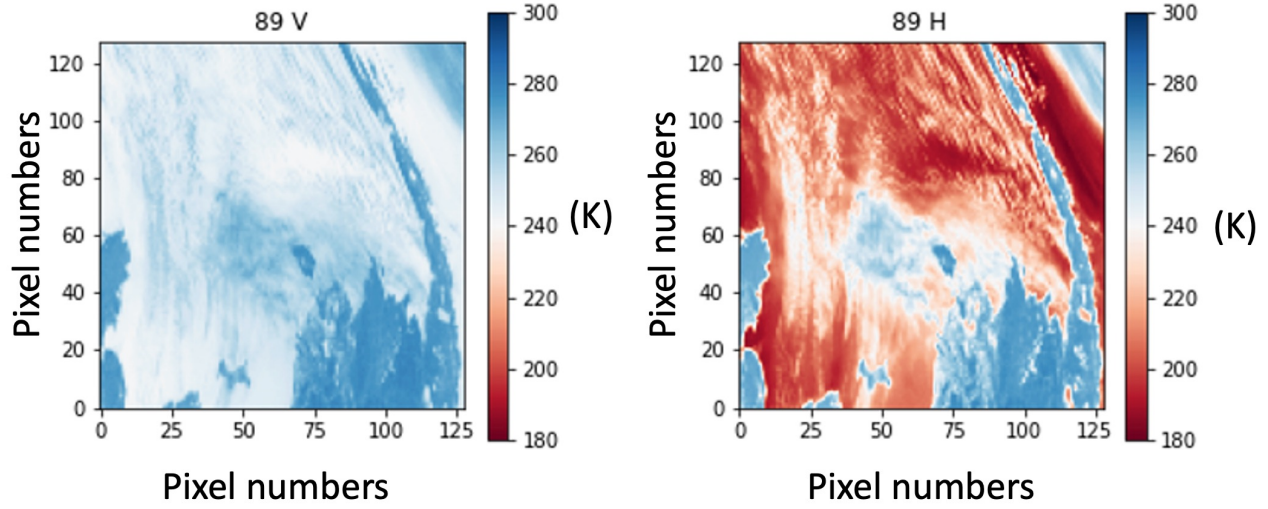

Figure 3. Vertical (89V) and horizontal (89H) polarisation of the 89-GHz channel brightness temperature in Kelvin from the GMI. The image is of 128 by 128 pixels representing roughly (1024 km by 1024 km).

Training dataset

- The training data set consists of 24 000 images for each domain, making 48 000 images in total.
- The observations are taken between 2015 and 2017.
- The validation set is made up of 4 000 images for each domain taken from the same period.
- These images contain 221 × 256 pixels and are chosen with the conditions that they either have at least 100 pixels with more than 10 mm/h rain or at least 10 pixels with more than 100 mm/h rain rates.

Results

Training loss

- As discussed previously, different learning rate schedules for each domain allow the losses of both domains to evolve in the same way and without a gap between them (figure 4). According to experiments, this could not be achieved if the learning rates for all networks involved have the same learning rate schedules.

Histogram of original and adapted data

- With test data consisting of two months of observation, including December 2018 and May 2020, figure 5 shows the comparison between the original normalized data and the adapted results.
- The original and adapted histograms are almost superimposed, though with some inaccuracy. Calculating the Kullback-Leiber divergence (Bishop et al., 1995) also confirms that there is more similarity between the original and adapted domain than without the transformation.

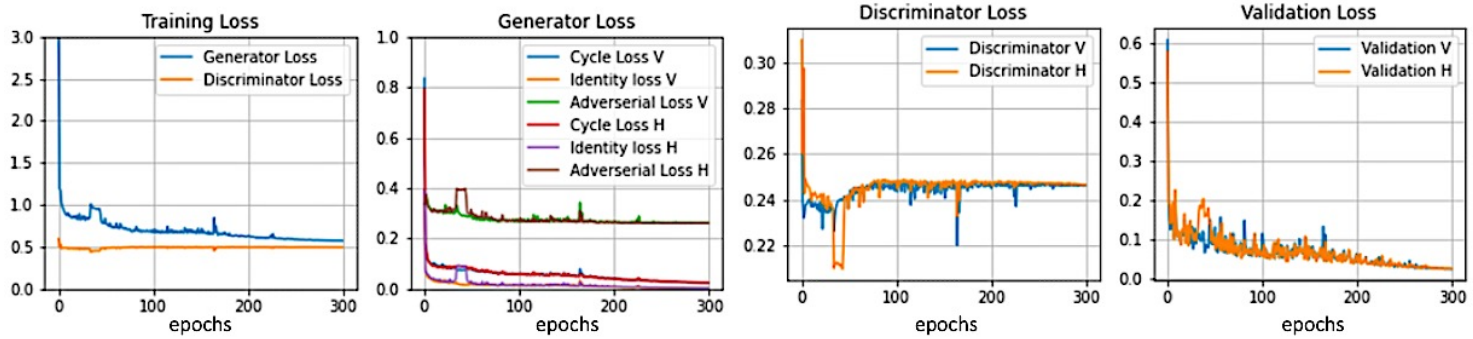

Figure 4. Training and validation losses for different components of the CycleGAN. The training loss (first plot) plot shows the generator and discriminator loss throughout training. Then, generator loss plot (second plot) and discriminator loss plot (third plot) show the details of each component. Finally, validation loss plot (fourth plot) shows the cycle-consistency and identity loss of each domain on validation dataset.

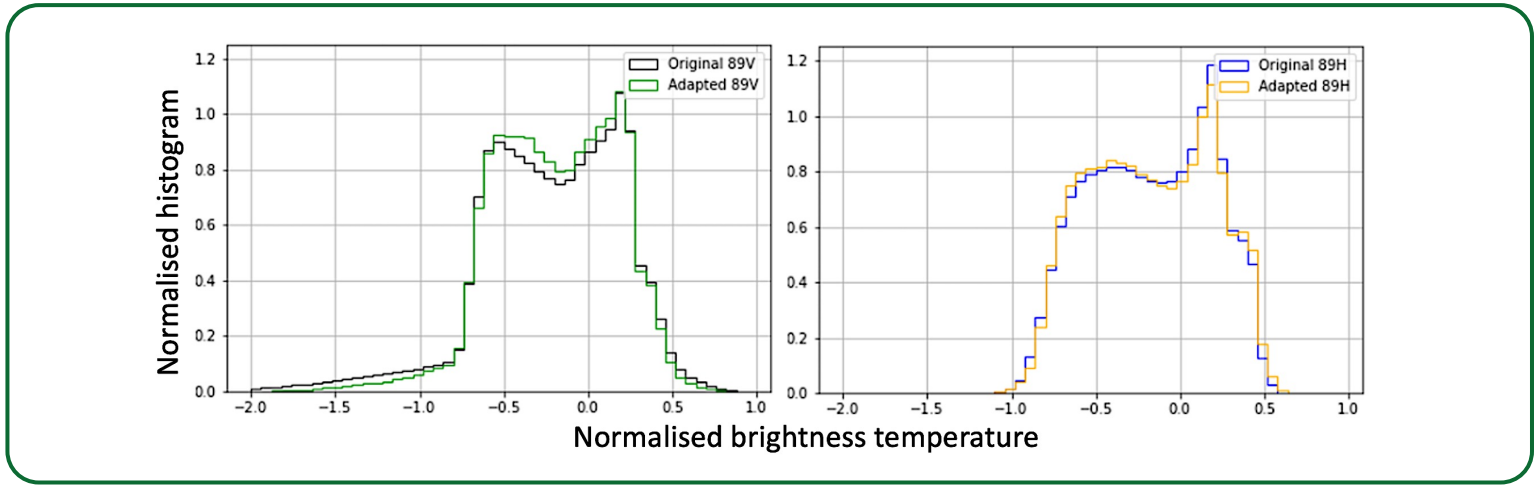

Figure 5. Comparison of the histogram of original 89V data and the adapted 89V data (left) and original 89H data and the adapted 89H (right).

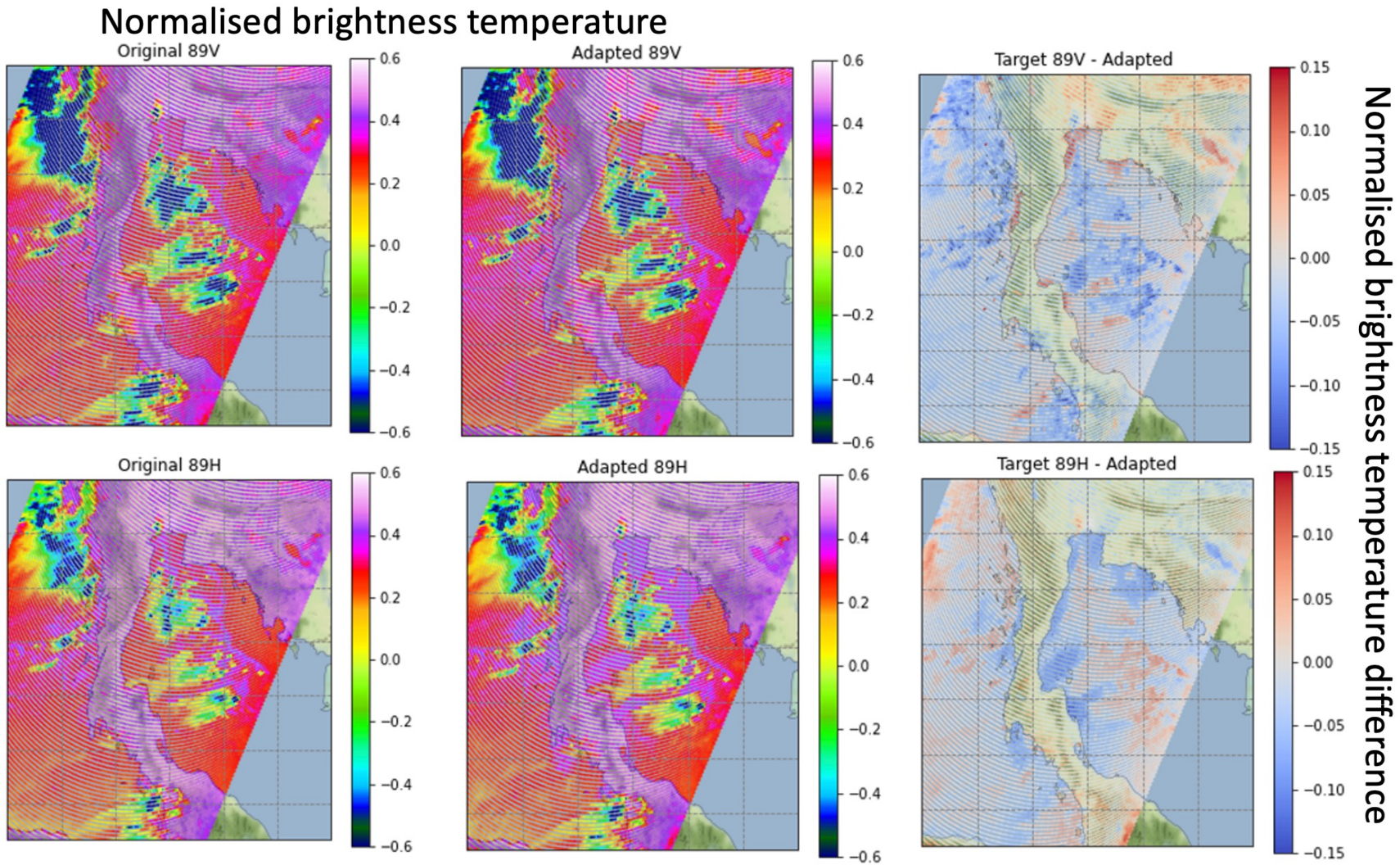

Figure 6. Original, adapted, and their difference of the 89-GHz channel observation from GMI on the 29th May 2017 with latitude 5-15° N and longitude 96-105° E (over parts of Thailand and Cambodia).

Results on adapted image

- Figure 6 shows the original satellite scans and the adapted images (89V adapted from 89H and 89H adapted from 89V) on a case study.
- CycleGAN can reproduce very well all the precipitation structures in the original images.
- However, in terms of values, there are differences in brightness temperature between the original and the adapted images that could not be picked up on qualitatively.

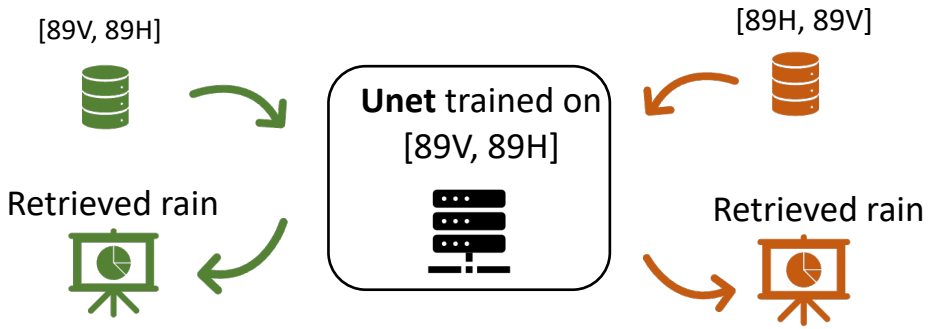

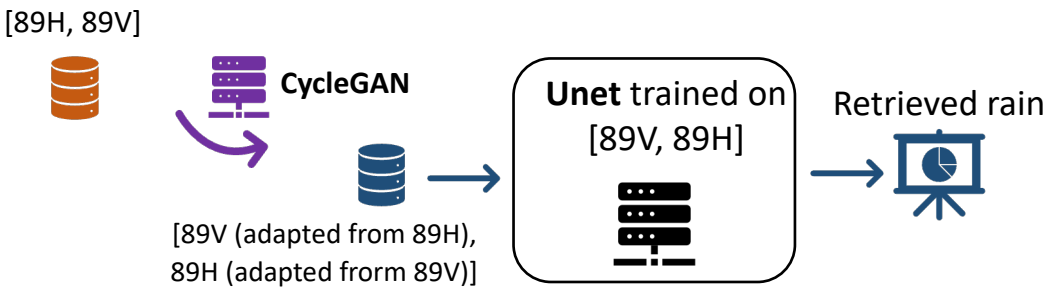

Case 1: the rain retrieval model trained on [89V, 89H] is tested on [89V, 89H] input data, the correct order on which it was trained → **ideal case scenario**.

Case 2: a rain retrieval model trained on [89V, 89H] inputs is tested on [89H, 89V] inputs (the order of inputs is reversed) → **worst case scenario**.

Case 3: the rain retrieval model is tested on the adapted brightness temperature, that is to say, the pair [89V (adapted from 89H), 89 H (adapted from 89V)] → **feasibility study**.

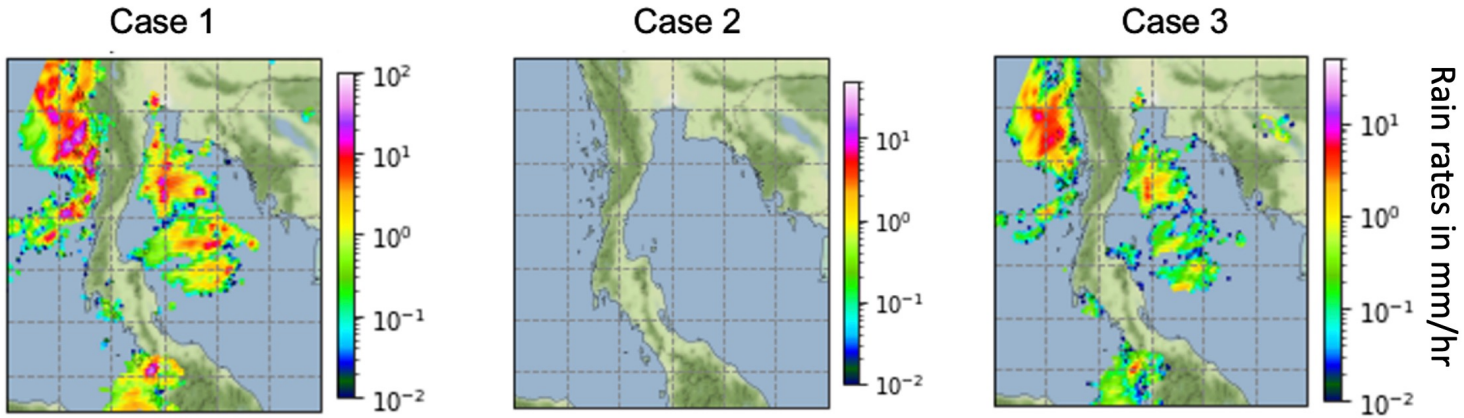

Figure 7. (Same observation as figure 6.) Comparison of retrieved surface rain rates in mm/h in Case 1 (left), Case 2 (middle), and Case 3 (right). The objective is to have case 3 as close to case 1 as possible. In the case study shown here, the rain rates retrieved from the adapted data (case 3) show the correct structure compared to case 1, albeit the lower intensity.

Conclusion

- The results from this toy experiment present a promising proof of concept. It also highlights the importance of quantitative assessment in image domain adaptation for a regression task.
- Based on the results presented, the pre-trained U-Net model is very sensitive to both the structure and, in turn, the gradient, as well as the value of the brightness temperature itself.
- The next step would be to study the real application with the GPM core observatory as the source domain and one of the satellites in the constellation, for example, SSMI/S, as the target domain.

References

- Bishop, C. M. et al. (1995). *Neural networks for pattern recognition*. Oxford university press.
- Goodfellow, I., Pouget-Abadie, J., Mirza, M., Xu, B., Warde-Farley, D., Ozair, S., Courville, A., and Bengio, Y. (2014). Generative adversarial nets. *Advances in neural information processing systems*, 27.
- Hou, A. Y., Kakar, R. K., Neeck, S., Azarbarzin, A. A., Kummerow, C. D., Kojima, M., Oki, R., Nakamura, K., and Iguchi, T. (2014). The global precipitation measurement mission. *Bulletin of the American Meteorological Society*, 95(5):701 – 722.
- Ronneberger, O., Fischer, P., and Brox, T. (2015). U-net: Convolutional networks for biomedical image segmentation. In *International Conference on Medical image computing and computer-assisted intervention*, pages 234–241. Springer.
- Viltard, N., Lepetit, P., Mallet, C., Barthès, L., and Martini, A. (2020). Retrieving rain rates from space borne microwave sensors using u-nets. In *Climate Informatics 2020. 10th International Conference*.
- Zhu, J.-Y., Park, T., Isola, P., and Efros, A. A. (2017a). Unpaired image-to-image translation using cycle-consistent adversarial networks. In *Proceedings of the IEEE international conference on computer vision*, pages 2223–2232.
- GPM Website: https://gpm.nasa.gov/missions/GPM/constellation